



ORIGINAL RESEARCH ARTICLE

Study on Microstructure and Mechanical Properties of AlCoCrFeNi High-Entropy Alloy Coating Prepared by Electroplating-Electron Beam Hybrid Cladding

Wenqin Wang, Wei Huang, Cuiyuan Lu , De Wang, Shen Li, and Ting Wang

Submitted: 1 January 2024 / Revised: 4 June 2024 / Accepted: 17 June 2024

The AlCoCrFeNi high-entropy alloy coatings with single matrix FCC phase and uniform distributions of elements were successfully synthesized on 304 stainless-steel substrate by a two-step surface modification method of electroplating and electron beam cladding, and the microstructure and mechanical properties of the coatings were studied and analyzed. The results indicate that the prepared AlCoCrFeNi high-entropy alloy coating has excellent mechanical properties, and its thickness increases with the increase of electron beam intensity. The highest hardness and elastic modulus of the coating reaches about 2.6 and 1.5 times those of the substrate, respectively, which are ascribed to increased Cr with less dilution from the substrate. The wear rate of the coating first decreases and then increases with increasing electron beam intensity. The best friction and wear properties are obtained in the coating with high hardness and few cracks prepared at an electron beam intensity of 6 mA. The main wear mechanisms of the coatings are abrasive wear and oxidation wear accompanied by slight adhesive wear.

Keywords AlCoCrFeNi high-entropy alloy coating, electroplating-electron beam hybrid cladding, mechanical properties, microstructure

1. Introduction

High-entropy alloys (HEAs) have become hot materials due to their advantages of uniform composition, dense microstructure, stable structure and great mechanical properties (Ref 1-4). HEAs usually consist of five or more major alloy elements, and among which, AlCoCrFeNi HEA is one of the most widely studied alloys owing to its high hardness, heat and corrosion resistance as well as friction and wear resistance (Ref 5-8). Thanks to those properties, it is desirable as a coating material.

Laser cladding is a common technology for preparing AlCoCrFeNi coating. It is a high-energy beam surface modification technology with characteristics of rapid heating and cooling within a small heat-affected zone area (Ref 9). Many researchers have applied this technique and successfully prepared AlCoCrFeNi coating on various steel substrates (Ref 10-15). Preparation of AlCoCrFeNi coating has been attempted by other techniques as well (Ref 16-18). Nevertheless, few research papers report on preparing AlCoCrFeNi coating by two commonly coating preparation methods, namely electron

beam cladding and electroplating. Similar to laser cladding, electron beam cladding is also characterized by rapid heating and cooling, and it can prevent oxidation of alloy coating due to its vacuum conditions (Ref 19). Zhao et al. (Ref 20) prepared AlCoCrFeNi coating on the surface of austenitic stainless-steel 253 MA by electron beam cladding and obtained a coating with hardness of 520 HV and wear resistance of more than double the substrate. Electroplating has the advantages of simple operation, low cost and uniform and dense coating of elements (Ref 21, 22). Rong et al. (Ref 23) prepared AlCoCrFeNi coating on the surface of copper alloy by electroplating and obtained hardness of 647 HV, which is four times that of the substrate.

However, different coating technologies have their own limitations. For instance, both laser cladding and electron beam cladding use high-energy and thus have the issue of high coating dilution rate, which leads to uneven distribution of elements/phase composition and affects the performance of the coating (Ref 24-26). Electroplating has the problem of poor bonding between the coating and substrate as well as difficulties of depositing elements (Ref 27, 28). In order to overcome the shortcomings of applying those coating preparation techniques alone and further improve the coating performance, researchers have attempted using combination of the techniques. For example, Wu et al. (Ref 29) prepared Ni-B-Ti coating on the surface of TA2 by electroplating and laser cladding and showed that the coating was well bonded to the substrate so that the coating's wear resistance was improved. Li et al. (Ref 30) prepared Ni-WC coating on the surface of TA2 by electroplating and electron beam cladding and also found that the coating had no obvious defects and was well bonded with the substrate. Although the above research of applying hybrid techniques of electroplating and high-energy beam cladding demonstrates great bonding between coating and

Wenqin Wang, Wei Huang, Cuiyuan Lu, and Shen Li, School of Advanced Manufacturing, Nanchang University, Nanchang 330031, China; De Wang, School of Aeronautical Manufacturing Engineering, Nanchang Hangkong University, Nanchang 330063, China; and Ting Wang, China Special Equipment Inspection and Research Institute, Beijing 100029, China. Contact e-mail: lucuiyuan@ncu.edu.cn.

substrate, they fail to tackle the problem of high dilution rate of coating caused by high-energy beam cladding.

Nevertheless, research on preparing AlCoCrFeNi HEA coating by hybrid techniques has not been reported. In this study, AlCoCrFeNi HEA coating is prepared on the surface of 304 stainless steel by electroplating and electron beam hybrid cladding, in which CoNi pre-coating is first fabricated on the substrate using electroplating, followed by preparing AlCoCrFeNi coating on the pre-coating by electron beam cladding. It is expected that the AlCoCrFeNi coating prepared on 304 stainless steel will take advantage of the high dilution rate of electron beam cladding instead since the Fe element in the substrate can be transmitted into the coating. The effects of process parameters on the microstructure and mechanical properties such as hardness, elastic modulus and wear resistance of the AlCoCrFeNi coatings are investigated, and the corresponding mechanisms are analyzed.

2. Experiment

2.1 Coating Preparation

The coating preparation was developed by two processes, namely electroplating and electron beam cladding, in which CoNi pre-coating and AlCoCrFeNi HEA coating were formed, respectively, after each process as shown in Fig. 1. In the electroplating process, the anode of the power supply was connected to a graphite plate, and the cathode of the power supply was connected to a 304 stainless-steel substrate. The compositions and concentrations of the plating solution and the electroplating parameters are presented in Table 1. In order to

improve the bonding strength between the coating and the substrate, the surface of the substrate was activated by an activating solution (160 mL/g H_2SO_4 and 80 mL/g H_2O_2). After the pre-coated sample was prepared, its surface was washed with alcohol.

In the electron beam cladding process, the pre-coated CoNi sample, Al and Cr sheets were fixed on the platform in the vacuum chamber of the equipment, and an electron beam was applied. The process parameters used in the electron beam cladding process are displayed in Table 2.

2.2 Microstructure and Properties Testing

The samples with AlCoCrFeNi coating were cut into two sizes ($5 \times 5 \times 10 \text{ mm}^3$ and $10 \times 10 \times 10 \text{ mm}^3$) for properties testing, in which the samples with size $5 \times 5 \times 10 \text{ mm}^3$ were used in the examination including morphology, phase and composition as well as hardness and elastic modulus measurements while the samples with size $10 \times 10 \times 10 \text{ mm}^3$ were used in the friction and wear tests. Before testing, the surface of the samples was polished. The morphology was examined by field emission scanning electron microscopy (FESEM, QUANTA 200F), the phase composition was determined by x-ray diffractometer (XRD, D8 Advance, Bruker) and element distribution was analyzed by energy-dispersive spectrometer (EDS).

The hardness and elastic modulus of AlCoCrFeNi coatings were measured by nanoindentation equipment (iMicro, Nanomechanics, USA) with a load of 100 mN and holding time of 10 s. Friction and wear properties were measured by a multifunctional friction and wear tester (UMT, TriboLab, USA) containing ZrO_2 grinding ball (diameter of 6 mm), in which load of 8 N was applied for 30 mins with rotation speed of 250

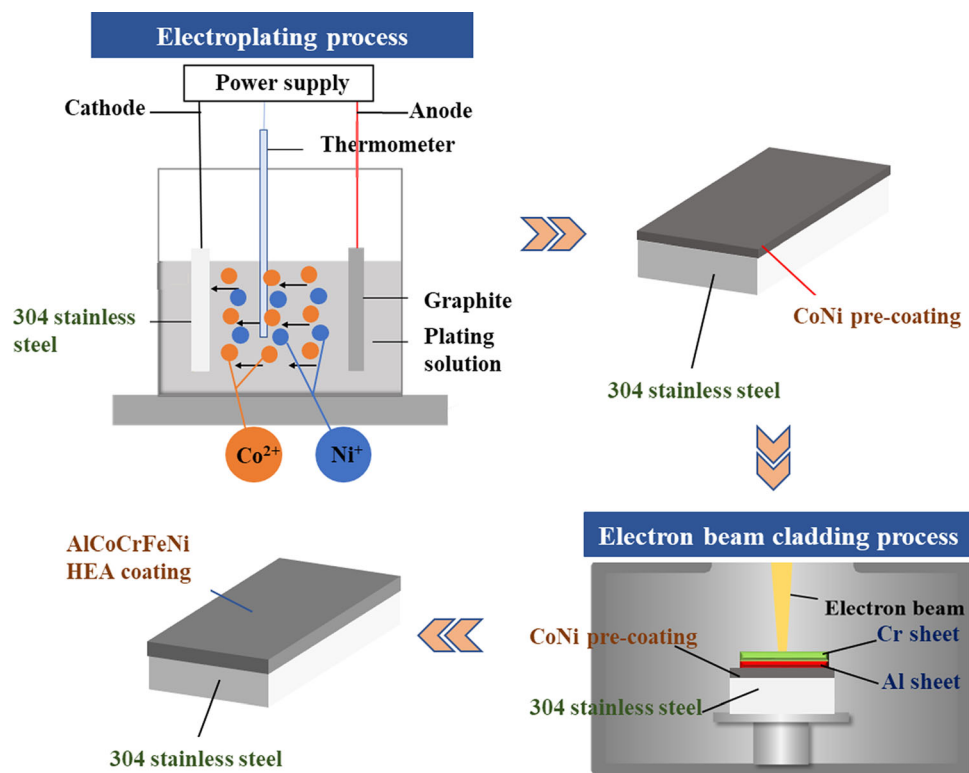


Fig. 1 Schematic plot of AlCoCrFeNi HEA coating preparation process

Table 1 Plating solution compositions and electroplating parameters

Solution compositions	Concentration, g/L	Electroplating parameters
NiCl ₂	30	Temperature: 60 °C
CoCl ₂	4	PH: 2.0
H ₃ BO ₃	20	Time: 60 min
NaCl	18	Cathode-current density: 10 A/dm ²
Na ₃ C ₆ H ₅ O ₇	30	
C ₆ H ₈ O ₇	30	
C ₇ H ₅ NO ₃ S	0.5	

Table 2 Process parameter settings used in the electron beam cladding process

Case	Voltage, kV	Spot diameter, mm	Scanning speed, mm/s	Electron beam intensity, mA
1	60	0.8	60	4
2				6
3				8

r/min and rotation radius of 3 mm. For accuracy, three samples with same experiment setting were measured for the above properties and the means were obtained.

3. Results and Analysis

3.1 Microstructure

The SEM observation results of the pre-coated CoNi alloy after electroplating and the AlCoCrFeNi coatings under three electron beam intensities are shown in Fig. 2(a), (b), (c) and (d), respectively. The average thicknesses of CoNi pre-coating and AlCoCrFeNi coatings at 4, 6 and 8 mA beam intensities are 16, 227, 278 and 458 μm , respectively, in which the AlCoCrFeNi coating is dramatically thicker than the CoNi pre-coating. The energy density can be used as indicator of the energy level of electron beam and is calculated with Eq 1 (Ref 31):

$$ED = \frac{U \cdot I}{v \cdot D} \quad (\text{Eq 1})$$

where ED represents energy density (J/mm^{-2}), U is voltage (kV), I is electron beam intensity (mA), v indicates scanning speed (mm/s) and D is spot diameter (mm). From Table 2 and Eq 1, the energy densities of three different beam intensities (4, 6 and 8 mA) are 5, 7.5 and 10 J/mm^{-2} , respectively. Figure 3 presents the relationship between coating thickness and ED, and it can be seen that the coating thickness increases more significantly as ED increases.

It can also be seen that there are through-wall cracks which extend vertically to the coating surface from the substrate-coating interface from Fig. 2(b) and (c). Furthermore, there are crack aggregations in Fig. 2(b), and the number of cracks in the coating decreases with increase of electron beam intensity by comparing Fig. 2(b), (c) and (d). As the dilution rate in the coating increases with the increase of electron beam intensity, it can be inferred that the increase of dilution rate plays a positive role in reducing the number of cracks in the AlCoCrFeNi coating.

In order to further study the element composition of AlCoCrFeNi coatings, EDS line and surface analysis were performed, respectively. Figure 4 displays line scanning images of the cross-section, indicating the change of element composition from the substrate to the coating. From Fig. 4, it can be seen that the elemental content distributions in both substrate and coating part of each specimen are relatively uniform. However, the elemental contents of Cr, Fe, and Al undergo relatively significant variations as shown by the step-mutational line changes from substrate to coating. There is notable decrease in Fe content while considerable increase in Cr content from substrate to coating. The increase of Al from substrate to the coating under electron beam intensity of 8 mA is not as large as the other conditions which may be due to the evaporation of Al under higher temperature. On the other hand, elemental contents of Co and Ni present relatively smooth transition from substrate to the coating. The results of EDS surface analysis also confirm that the distributions of elements in the coatings under three electron beam intensities are relatively uniform. Table 3 shows the average and standard deviation of atomic percentage of each element in the AlCoCrFeNi coatings. From both Table 3 and Fig. 4, it can be seen that the proportion of Cr element at electron beam intensity of 6 mA is higher while the proportion of Fe element at electron beam intensity of 8 mA is higher. The reasons may be the following: The melting point of Cr is relatively high (1857°C) (Ref 32), and as the electron beam intensity increases from 4 to 6 mA, Cr sheets gradually melt, and thus, the proportion of Cr element in the coating increases. However, as the electron beam intensity continues increasing to 8 mA, the obtained energy is high enough so that the Cr sheets have melted completely and the energy is also absorbed by the substrate. As a result, the dilution rate of the coating increases, which leads to the increased proportion of Fe element from the substrate while decreased proportion of Cr element in the coating.

Figure 5 displays the XRD patterns of AlCoCrFeNi coatings under three different electron beam intensities. It can be seen from Fig. 5 that the phase composition of coating is single matrix FCC phase, and there are no complex phases of other

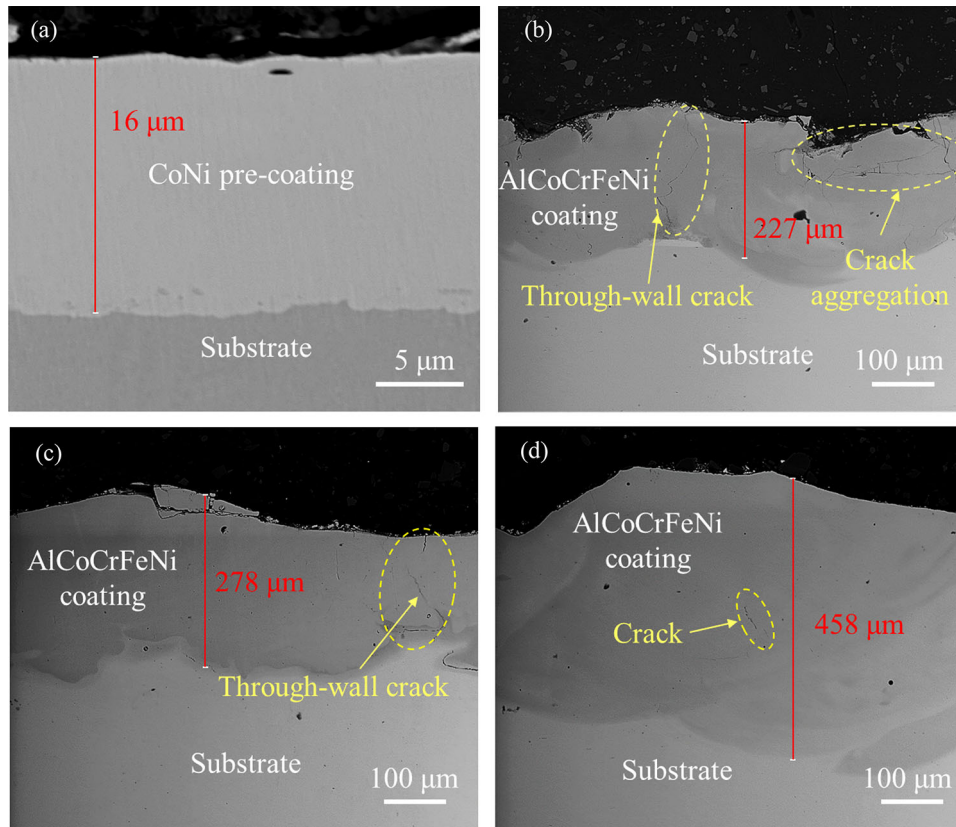


Fig. 2 SEM of cross-sectional morphology of (a) CoNi pre-coating and AlCoCrFeNi coating under three electron beam intensities: (b) 4 mA, (c) 6 mA and (d) 8 mA

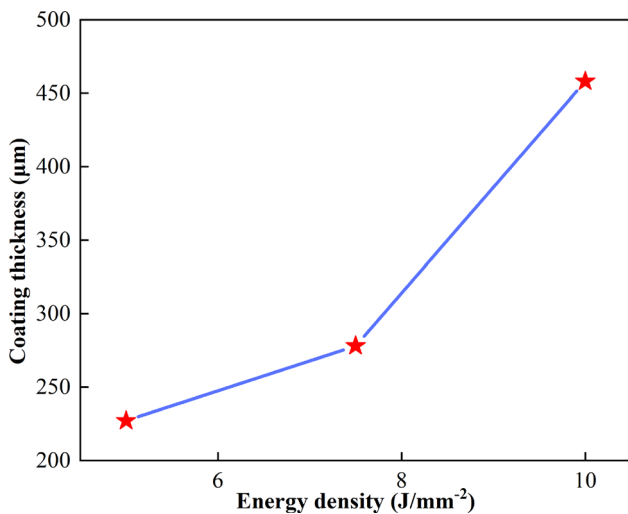


Fig. 3 The relationship between AlCoCrFeNi coating thickness and energy density of electron beam

intermetallic compounds under all three cases. The causes may be twofold; on the one hand, the high-entropy effect hinders the formation of intermetallic compounds (Ref 33), and on the other hand, the low Al content in the coatings promotes the formation of single FCC phase (Ref 34, 35).

3.2 Hardness and Elastic Modulus

Figure 6 displays the nanoindentation results of the cross-sections of the AlCoCrFeNi coatings under three cases of electron beam intensities. It can be seen from Fig. 6(a) that the hardness of coating decreases in general with increased distance from the surface under electron beam intensity of 4 mA. The cause of such phenomena is that there is more dilution effect in the coating when it gets closer to the substrate. However, at electron beam intensity of 6 mA, the hardness of coating increases with increase of depth from surface to maximum of 1051 HV and then decreases. According to the line scanning image of Fig. 4(b), the increase of hardness with increased depth from the surface may be caused by more Cr diffusing toward the substrate given the increased energy obtained, while the decrease of hardness with further increased depth from surface is due to increased dilution effect from the substrate which counteracts the effect of increased Cr diffusion. When the electron beam intensity reaches 8 mA, the hardness of coating also decreases overall as the distance to the surface increases. This is attributed to another fact that Cr sheet fully melts into the coating and the effect of dilution from the substrate dominates under highest energy. Since the dilution is more toward substrate, there is a general decrease of hardness as depth from the surface increases.

It can be seen from Fig. 6(b) that the changes of elastic modulus with respect to the depth from the coating surface are

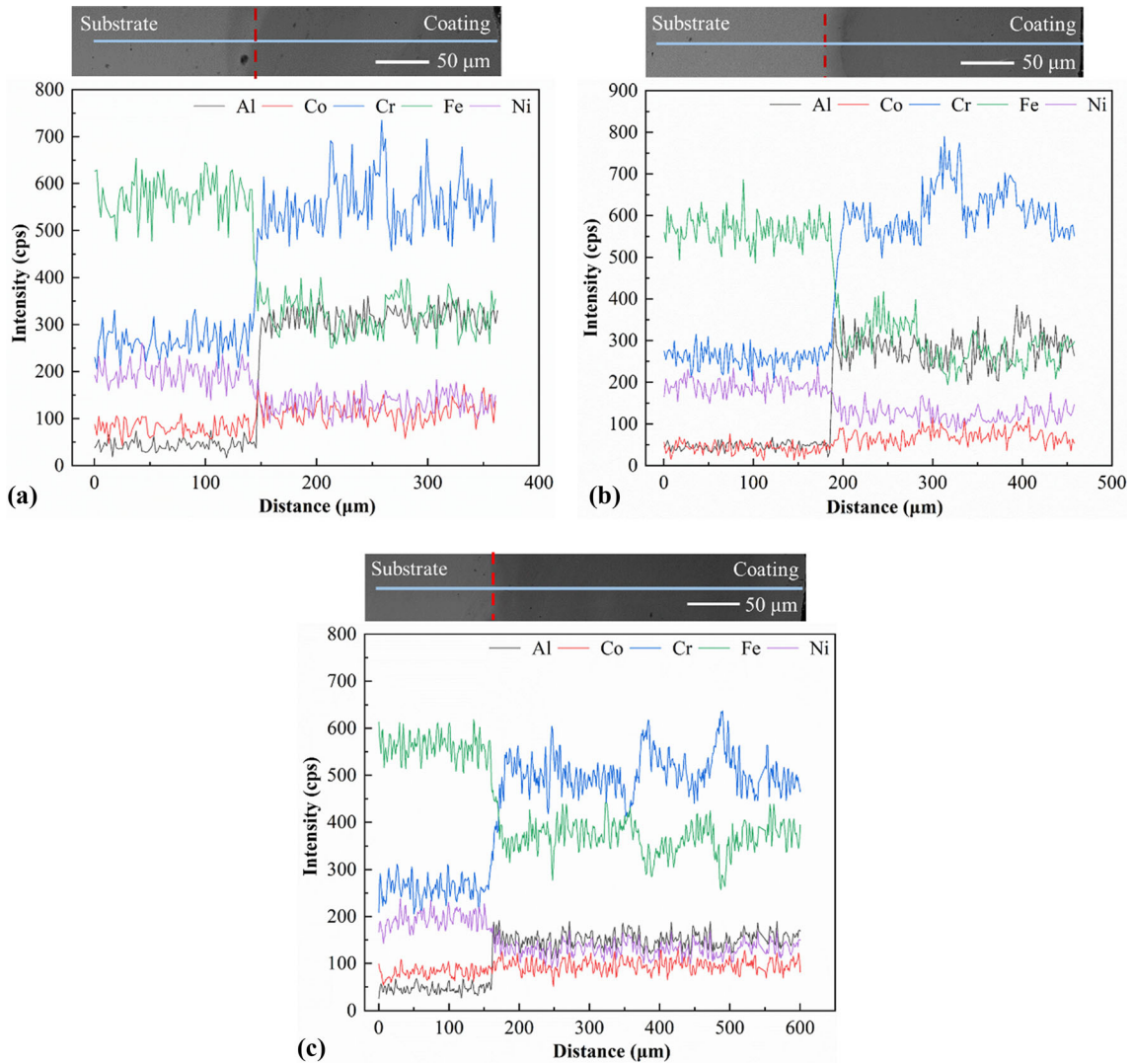


Fig. 4. Line scanning images of the cross-section of AlCoCrFeNi coatings under different electron beam intensities: (a) 4 mA, (b) 6 mA and (c) 8 mA

Table 3 The average and standard deviation of the atomic percentage of each element in the AlCoCrFeNi coatings (at %)

Beam intensity	Al	Co	Cr	Fe	Ni
4 mA	15.4 ± 1.2	2.8 ± 0.2	52.6 ± 2.1	18.5 ± 2.5	10.7 ± 1.5
6 mA	8.2 ± 0.7	0.7 ± 0.1	78.4 ± 1.2	8.5 ± 0.8	4.2 ± 0.3
8 mA	12.6 ± 0.6	1.3 ± 0.2	41.5 ± 0.9	35.3 ± 1.3	9.3 ± 0.4

similar to that of the hardness, except that the elastic modulus drops more significantly within 0.15-0.2 mm from the surface under electron beam intensity of 4 mA, which may be derived from aggregation of cracks in the area (see Fig. 2(b)).

In Fig. 6(c), the average hardness of coatings under electron beam intensities of 4, 6, 8 mA and the substrate is 650, 944, 860 and 363 HV, respectively, in which the average hardness of coatings is about 1.8-2.6 times that of the substrate. Similarly in Fig. 6(d), the average elastic modulus of coatings under electron beam intensities of 4, 6, 8 mA and the substrate is 256, 299, 260 and 194 GPa, respectively, and thus, the average

elastic modulus of coatings is roughly 1.3-1.5 times that of the substrate. In summary, both hardness and elastic modulus of coatings improve obviously compared with the substrate. Besides, it can be seen from Fig. 6(c) and (d) that the average hardness and elastic modulus of coatings increase first and then decrease as the intensity of electron beam increases. The following two factors may be responsible for such change behaviors: (1) When the electron beam intensity increases from 4 to 6 mA, the hardness and elastic modulus increase due to increased melting of Cr sheets, (2) when the electron beam intensity further increases to 8 mA, Cr sheets fully melt while

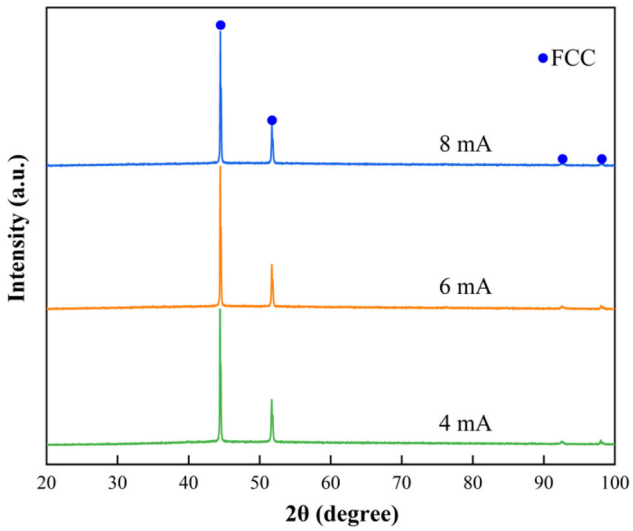


Fig. 5 XRD pattern of AlCoCrFeNi coatings under different electron beam intensities

the dilution rate of the substrate keeps increasing, which results in the decrease of hardness and elastic modulus.

In order to further demonstrate the advantages of the aforementioned AlCoCrFeNi coating, the comparisons among the hardness of AlCoCrFeNi coatings prepared in this work and earlier which adopt only high-energy beam cladding or electroplating (Ref 10-15, 19, 20, 23) are provided in Fig. 7. It can be seen that the hardness of AlCoCrFeNi coatings prepared under 6 mA and 8 mA electron beam intensities from this work is above 800 HV, which are much higher than the results from literature. In addition, even the smallest hardness of AlCoCrFeNi coating obtained in this work is higher than the approximate average hardness (600 HV) of that coating from literature. Hence, the AlCoCrFeNi coatings prepared in this work exhibit outstanding hardness, and it can thus be concluded that the preparation of AlCoCrFeNi coating by electroplating-electron beam hybrid cladding technique outperforms using only high-energy cladding or electroplating.

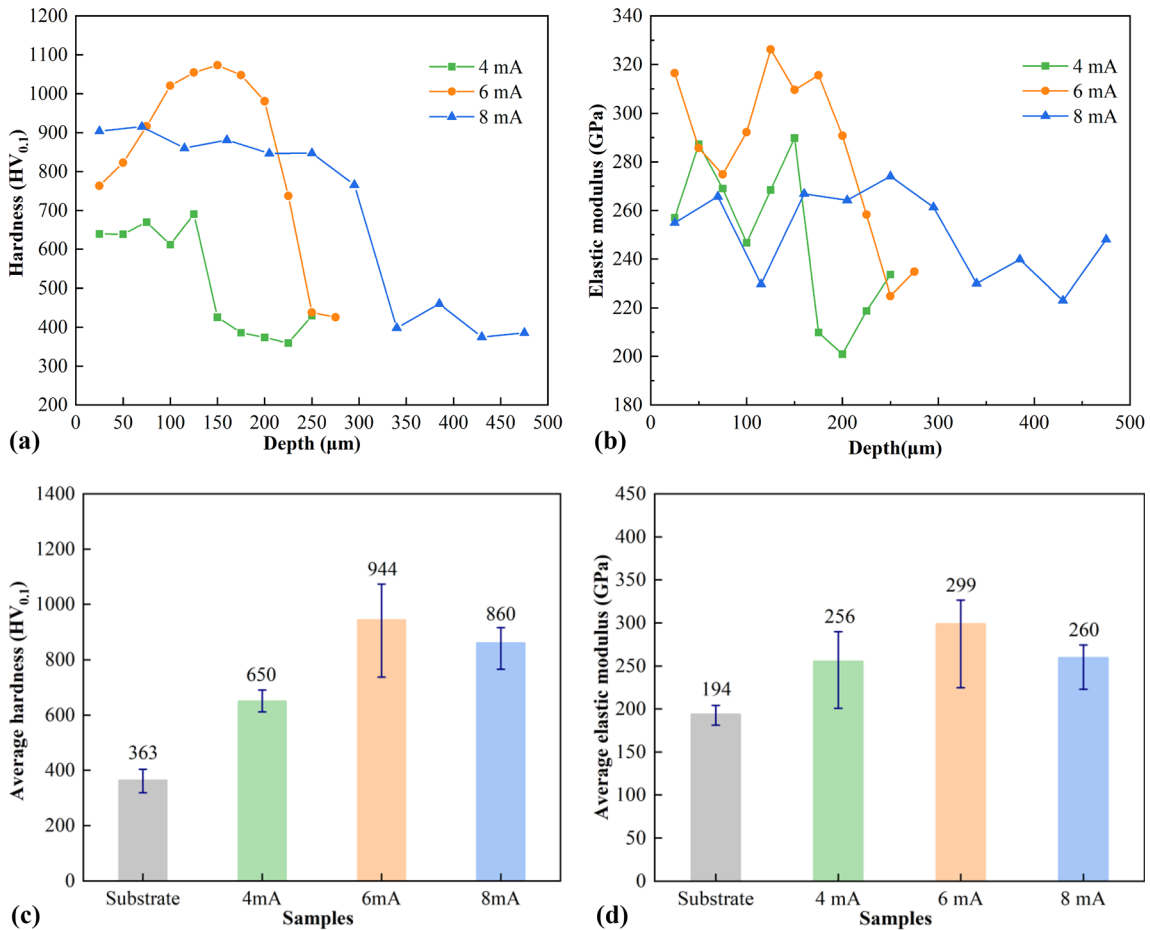


Fig. 6 Nanoindentation results of AlCoCrFeNi coatings: (a) Vickers hardness and (b) elastic modulus at different depths from surface, (c) average hardness and (d) average elastic modulus

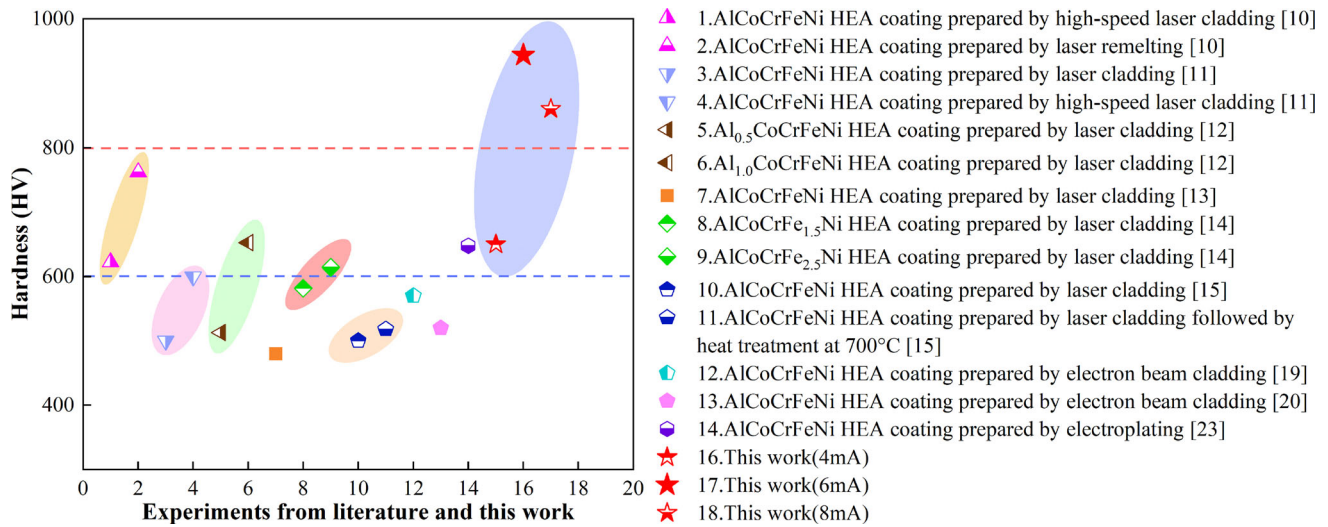


Fig. 7 Summary of hardness of AlCoCrFeNi coatings prepared by different techniques in literature and this work

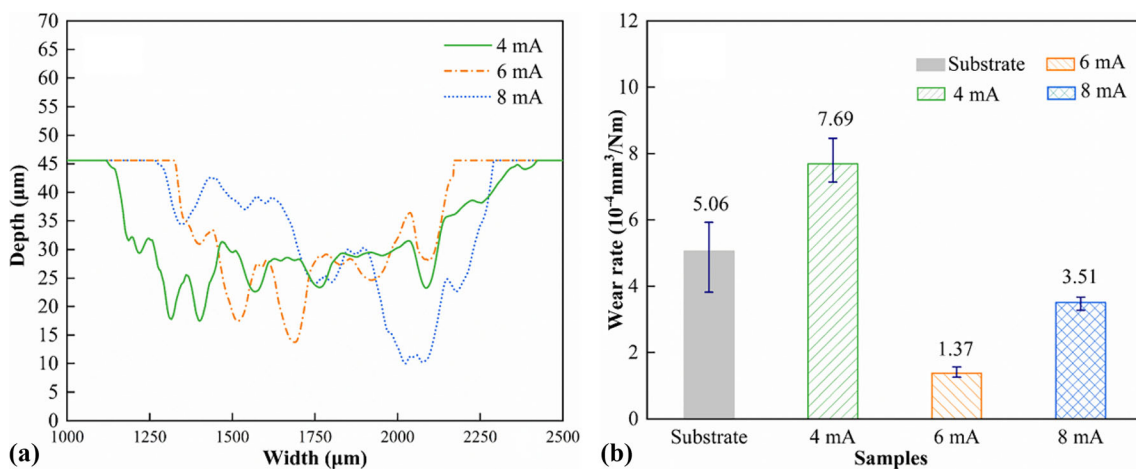


Fig. 8 (a) Wear profiles of AlCoCrFeNi coatings and (b) wear rates of AlCoCrFeNi coatings and the substrate

3.3 Friction and Wear Properties

3.3.1 Friction Coefficient and Wear Rate. Figure 8(a) presents the wear profile curves of coatings prepared under different electron beam intensities from the friction and wear experiments. It can be seen that the wear width of coating prepared at 6 mA electron beam intensity is the smallest and the wear depth is less fluctuated, which implies the coating owns better wear resistance. Figure 8(b) displays the wear rate bar charts derived from Fig. 8(a). It can be seen that the wear rate of coating decreases first and then increases with increase of electron beam intensity (see Fig. 8b). By comparing Fig. 6(c), the higher the hardness is, the lower the wear rate is, which is consistent with the Archard wear theory, stating that the wear

volume or mass loss of a material is inversely proportional to the hardness of the softer material involved in the contact (Ref 36). Hence, hardness has a positive effect in improving wear resistance. Besides, it can be seen that the wear rates of coatings prepared at beam intensities of 6 and 8 mA are lower than that of the substrate. It is noted that although the hardness of coating under 4 mA electron beam intensity is higher than the substrate (see Fig. 6c); its wear rate is higher than the substrate (see Fig. 8b), which may be due to the existence of crack aggregations (see Fig. 2b).

3.3.2 Wear Mechanism. The surface morphologies of coatings after friction and wear experiment are observed by SEM. It can be seen from Fig. 9(a), (b) and (c) that the wear widths of coatings prepared at electron beam intensities of 4, 6

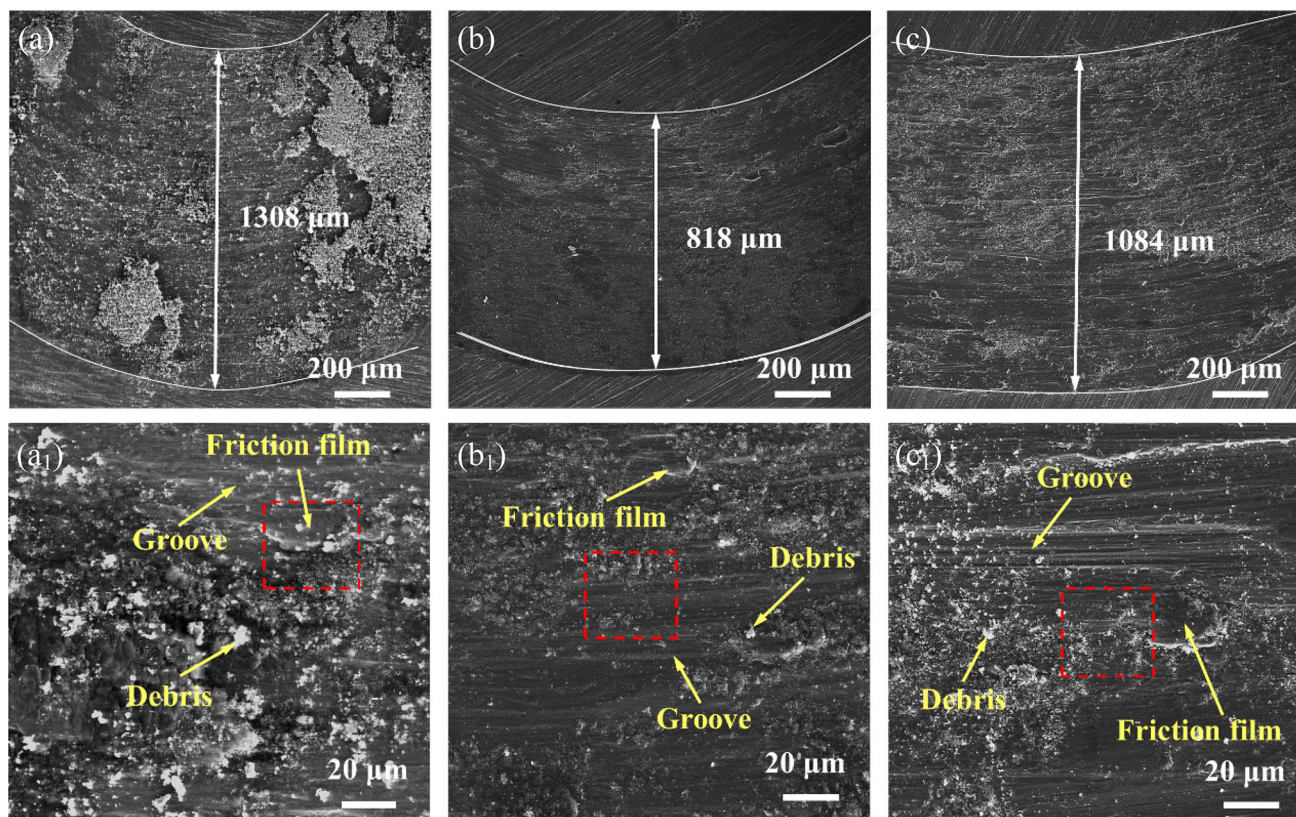


Fig. 9 Wear morphology of AlCoCrFeNi coatings: (a) 4 mA, (b) 6 mA and (c) 8 mA

and 8 mA are 1308, 818 and 1084 μm , respectively. It demonstrates that the wear is most serious when the electron beam intensity is 4 mA, which is consistent with the results from Fig. 8. In Fig. 9(a₁-c₁), a large number of debris and grooves are found on the wear surface from all cases, among which the debris and grooves generated under electron beam intensity of 6 mA are much less, which matches the wear rate results from Fig. 8(b). Since debris and grooves are typical characteristics of abrasive wear, it can thus be concluded that the wear mechanism of coating includes abrasive wear (Ref 12, 20). In addition, it is also observed that the friction film is formed by accumulation of wear debris after repeated extrusion by the grinding ball. The friction film has protective effect on the coating surface (Ref 12).

Figure 10 presents zoomed images of the area inside the red frame in Fig. 9(a₁-c₁) and the corresponding EDS results. In Fig. 10(c), spalling pits are formed due to plastic deformation and work hardening of the coating, indicating slight adhesive wear (Ref 13, 20). EDS analysis shows that O element is mainly concentrated in the wear debris area, which implies the occurrence of oxidization behavior in wear debris. The points in non-wear debris (points 1, 3, 5) and the points in wear debris (points 2, 4, 6) of three cases are then selected for EDS point analysis, and the analysis results are displayed in Table 4. It can be seen that O contents in wear debris points are significantly higher than those in non-wear debris points, which further proves the existence of oxidative wear in the coating. By comparing Fig. 10(a), (b) and (c), coating at electron beam intensity of 4 and 6 mA presents the highest and lowest oxidation degree, respectively. According to the wear rate results from Fig. 8(b), it can be inferred that the more the

oxidation degree of the coating is, the more serious the wear is. In consequence, it can be concluded that multiple wear mechanisms exist in the wear process, in which the main wear mechanisms of the coatings are abrasive wear and oxidation wear while accompanied by slight adhesive wear.

Based on the above results and analysis, the friction and wear process can be summarized in three phases as shown in Fig. 11. In phase 1, a few debris particles appear on the coating surface due to the repeated friction of ZrO₂ grinding balls. In phase 2, further friction causes plastic deformation and work hardening of the coating resulting in increased number of wear debris and spalling pits. In addition, due to the sliding of abrasive particles under the action of grinding balls, grooves appeared on the surface of the coating. In phase 3, the wear debris is repeatedly squeezed by the grinding ball and accumulates, resulting in formation of friction film.

4. Conclusions

The AlCoCrFeNi HEA coatings with high mechanical properties were successfully prepared on the surface of 304 stainless steel by electroplating and electron beam hybrid cladding in this paper, the microstructure and mechanical properties including hardness, elastic modulus and wear resistance of the coatings under three different electron beam intensities were studied, and corresponding mechanisms were analyzed. The main findings are summarized:

- (1) With the assistance of the dilution of Fe element from the substrate, the AlCoCrFeNi coating with single ma-

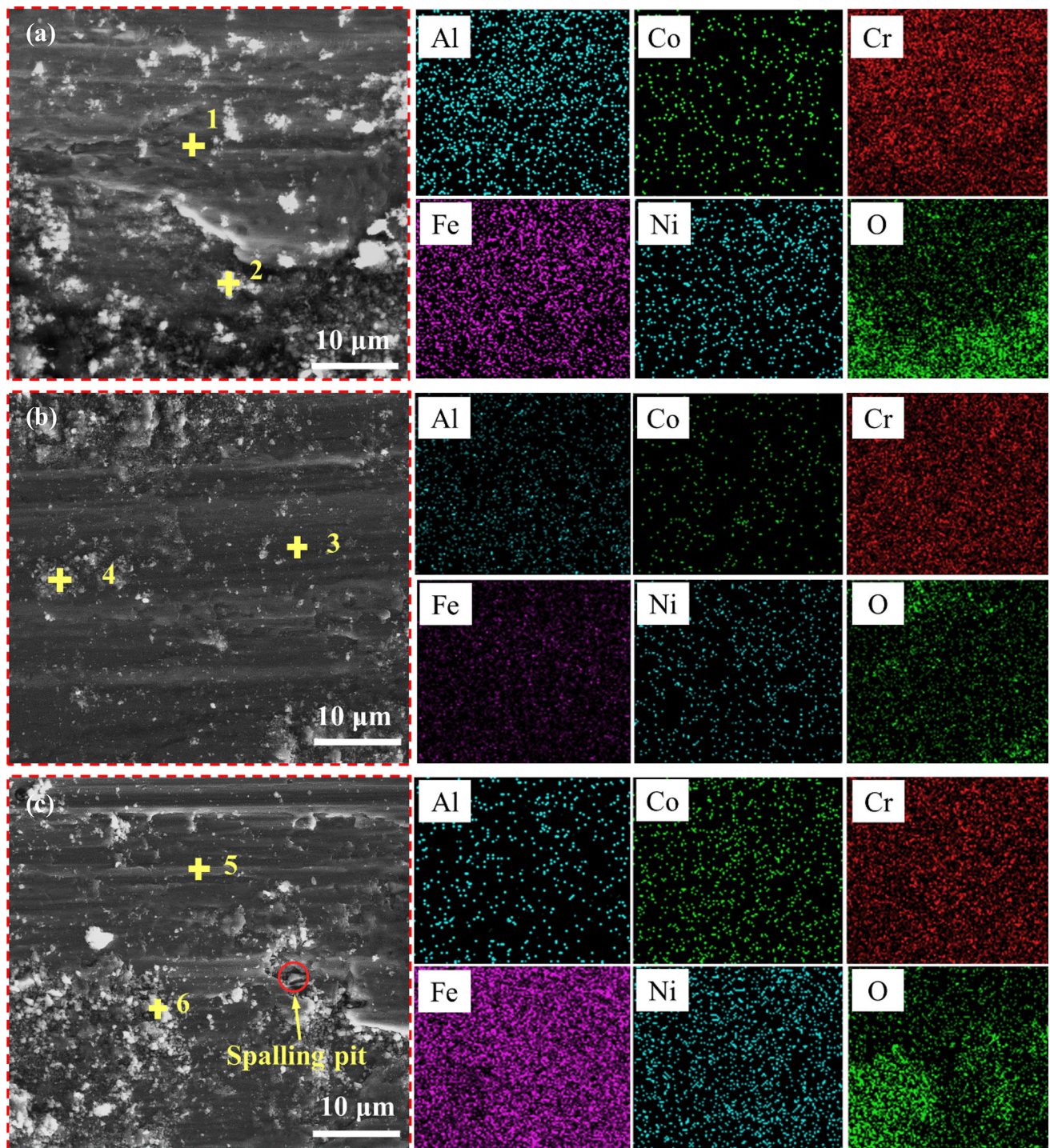


Fig. 10 Zoomed images of the area inside the red frame in Fig. 9 and EDS surface analysis of AlCoCrFeNi coatings: (a) 4 mA, (b) 6 mA and (c) 8 mA

trix FCC phase and uniform element distributions can be prepared on the surface of 304 stainless steel by electroplating and electron beam hybrid cladding, and the thickness of the coating increases as electron beam intensity increases.

- (2) The hardness and elastic modulus of AlCoCrFeNi coatings prepared by different electron beam intensities are about 1.8-2.6 times and 1.3-1.5 times of those of the

substrate, respectively. The optimal hardness and elastic modulus of the coatings are owing to the highest proportion of Cr element. The obtained hardness outperforms that of the AlCoCrFeNi coatings prepared by single coating techniques reported in earlier literature.

- (3) The wear rate of AlCoCrFeNi coating decreases first and then increases with increasing electron beam intensity. The coating prepared at electron beam intensity of

Table 4 EDS point analysis of six selected points from Fig. 10 (at %)

Points	Al	Co	Cr	Fe	Ni	O
Point 1	6.4	0.4	43.1	15.5	3.9	30.8
Point 2	3.6	0.2	24.5	8.3	1.6	62.0
Point 3	8.3	0.0	46.7	29.5	4.6	11.0
Point 4	4.8	0.5	38.9	16.9	2.4	36.0
Point 5	0.3	0.0	17.7	62.0	6.3	13.7
Point 6	0.1	0.1	9.8	31.5	3.4	55.2

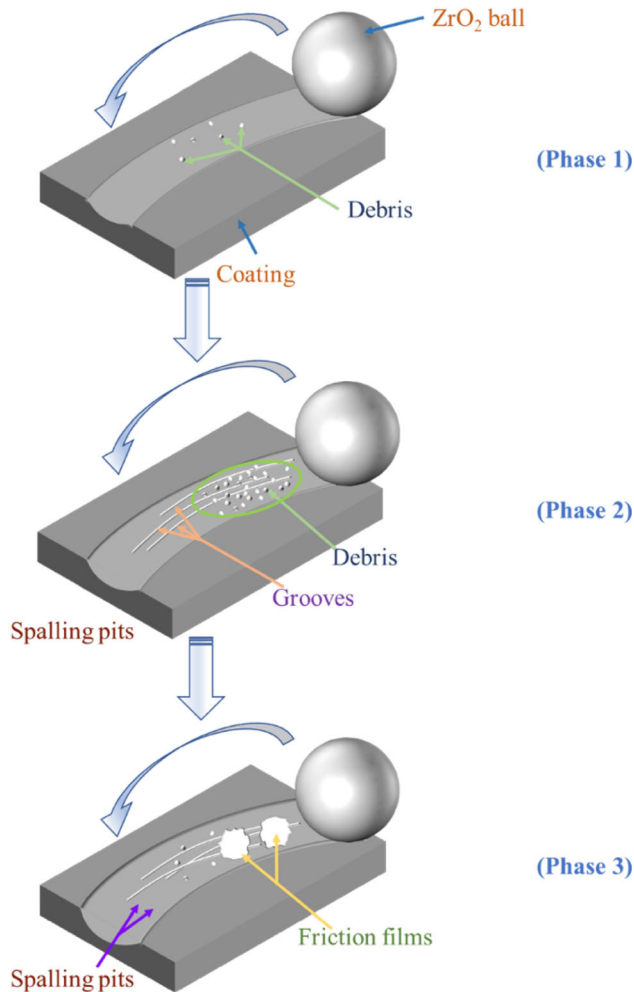


Fig. 11 Schematic diagram of friction and wear process

6 mA exhibits the lowest wear rate of 1.37×10^{-4} mm³/(Nm) due to high hardness and few cracks in the coating.

- (4) The friction and wear process of the AlCoCrFeNi coatings can be ordered in three phases: formation of a few wear debris and development of large amount wear debris as well as spalling pits and grooves and generation of friction film. The main wear mechanisms of the coatings are abrasive wear and oxidation wear accompanied by slight adhesive wear.

Acknowledgments

This work was supported by the National Natural Science Foundation of China (52205375), Jiangxi Provincial Natural Science Foundation [20232BAB214001, 20232BAB204049, jxsq2 019201118], Innovation Fund for Fostering Young Talents of Nanchang University (PYQN20230077) and 2023 Ganpo Talents Support Program-High level and Urgently Needed Oversea Talents Program (20232BCJ25074).

References

- X. Li, Y.Q. Wang, J.Y. Zhang et al., Research progress of high entropy alloy coatings, *Surf. Technol.*, 2023, **52**(01), p 1–20.
- C.M. Yang, X.B. Liu, Y.F. Liu et al., Effect of Cu-doping on tribological properties of laser-cladded FeCoCrNiCu_x high-entropy alloy coatings, *Tribol. Int.*, 2023, **188**, 108868
- M. Dehestani, S. Sharafi and G.R. Khayati, The effect of pulse current density on the microstructure, magnetic, mechanical, and corrosion properties of high-entropy alloy coating FeCoNiMoW, achieved through electro co-deposition, *Intermetallics*, 2022, **147**, 107610
- J. Yang, C. Wang, L. Zhang et al., Microstructure evolution and properties of Fe-Ni-Cr-Co-Mo-W high-entropy alloy coatings by plasma surface alloying technology, *Surf. Coat. Technol.*, 2023, **467**, 129732
- F. Kaya, M. Yetiş, G.İ Selimoğlu et al., Influence of Co content on microstructure and hardness of AlCo_xCrFeNi (0 ≤ x ≤ 1) high-entropy alloys produced by self-propagating high-temperature synthesis, *Eng. Sci. Technol. Int. J.*, 2022, **27**, 101003
- G. Qin, W. Xue, C. Fan et al., Effect of Co content on phase formation and mechanical properties of (AlCoCrFeNi)_{100-x}Co_x high-entropy alloys, *Mater. Sci. Eng. A*, 2018, **710**, p 200–205.
- T. Xiong, S.J. Zheng et al., High-strength and high-ductility AlCoCrFeNi_{2.1} eutectic high-entropy alloy achieved via precipitation strengthening in a heterogeneous structure, *Scripta Mater.*, 2020, **186**, p 336–340.
- X.K. Zhang, T.H. Chou, W.P. Li et al., Microstructure and mechanical properties of (FeCoNi)_{100-x}(NiAl)_x eutectic multi-principal element alloys, *J. Alloy. Compd.*, 2021, **862**, 158349
- Z. Gao, L. Wang, Y. Wang et al., Crack defects and formation mechanism of FeCoCrNi high entropy alloy coating on TC4 titanium alloy prepared by laser cladding, *J. Alloy. Compd.*, 2022, **903**, 163905
- Z. Chong, Y. Sun, W. Cheng et al., Laser remelting induces grain refinement and properties enhancement in high-speed laser cladding AlCoCrFeNi high-entropy alloy coatings, *Intermetallics*, 2022, **150**, 107686
- Z. Chong, Y. Sun, W. Cheng et al., Enhanced wear and corrosion resistances of AlCoCrFeNi high-entropy alloy coatings via high-speed laser cladding, *Mater. Today Commun.*, 2022, **33**, 104417
- Z. Li, C. Jing, Y. Feng et al., Phase evolution and properties of Al_xCoCrFeNi high-entropy alloys coatings by laser cladding, *Mater. Today Commun.*, 2023, **35**, 105800
- X. Wei, P. Zhang, Z. Yu et al., Effect of phase transformation on mechanical properties of Al_{16.80}Co_{20.74}Cr_{20.49}Fe_{21.28}Ni₂₀₇₀ high entropy alloy coatings processed by laser cladding, *J. Alloys Compd.*, 2021, **862**, p 158563.
- G.J. Zhang, Q.W. Tian, K.X. Yin et al., Effect of Fe on microstructure and properties of AlCoCrFeNi (x=1.5, 2.5) high entropy alloy coatings prepared by laser cladding, *Intermetallics*, 2020, **119**, p 106722.
- W. Guo, N. Ding, G. Liu et al., Microstructure evolution of a multi-track AlCoCrFeNi high entropy alloy coating fabricated by laser cladding, *Mater. Charact.*, 2022, **184**, 111660
- Q. Fan, C. Chen, C. Fan et al., Ultrasonic induces grain refinement in gas tungsten arc cladding AlCoCrFeNi high-entropy alloy coatings, *Mater. Sci. Eng. A*, 2021, **821**, 141607
- A. Meghwal, S. Singh, A. Anupam et al., Nano- and micro-mechanical properties and corrosion performance of a HVOF sprayed AlCoCrFeNi high-entropy alloy coating, *J. Alloy. Compd.*, 2022, **912**, 165000

18. J.T. Liang, K.C. Cheng, Y.C. Chen et al., Comparisons of plasma-sprayed and sputtering Al_{0.5}CoCrFeNi₂ high-entropy alloy coatings, *Surf. Coat. Technol.*, 2020, **403**, p 126411.
19. A.A. Ruktuev, D.V. Lazurenko, T.S. Ogneva et al., Structure and oxidation behavior of CoCrFeNiX (where X is Al, Cu, or Mn) coatings obtained by electron beam cladding in air atmosphere, *Surf. Coat. Technol.*, 2022, **448**, 128921
20. G. Zhao, Y. Zhang, H. Zhao et al., Study on the process optimization and wear resistance of electron beam cladding AlCoCrFeNi coating on 253MA austenitic stainless steel surface, *Mater Charact*, 2023, **205**, 113341
21. Q. Wan, B.Y. Jia, P. Liu et al., Microstructure and mechanical properties of FeCoCrNiAl_{0.1}N high entropy alloy nitride coatings synthesized by cathodic arc ion plating using alloy target, *Surf. Coat. Technol.*, 2023, **457**, p 129305.
22. D.V. Sidelev, C. Poltronieri, M. Bestetti et al., A comparative study on high-temperature air oxidation of Cr-coated E110 zirconium alloy deposited by magnetron sputtering and electroplating, *Surf. Coat. Technol.*, 2022, **433**, 128134
23. Z. Rong, C. Wang, Y. Wang et al., Microstructure and properties of FeCoNiCrX (X Mn, Al) high-entropy alloy coatings, *J. Alloy. Compd.*, 2022, **921**, 166061
24. D. Xu, H. Wang, X. Tao et al., Investigation on microstructure, hardness and wear resistance of electron beam wire-feeding deposited Inconel 718 alloy coatings, *Met. Mater. Int.*, 2021, **27**, p 1263–1272.
25. R. Müller, P. Hengst, H. Biermann et al., Development of a basic technology for multilayer electron beam cladding of Inconel 718 nickel-based alloy onto an austenitic stainless steel, *CIRP J. Manuf. Sci. Technol.*, 2022, **38**, p 84–92.
26. J. Cai, Y. Yao, C. Gao et al., Comparison of microstructure and oxidation behavior of NiCoCrAlYSi laser cladding coating before and after high-current pulsed electron beam modification, *J. Alloy. Compd.*, 2021, **881**, 160651
27. D. Xu, S. Ni, Y. Bu et al., Electrodeposition of high-quality Cr coatings with solid solution Al from Cr²⁺ electrolyte, *Surf. Coat. Technol.*, 2023, **452**, 129121
28. A. Endo, M. Miyake and T. Hirato, Electrodeposition of aluminum from 1,3-Dimethyl-2-Imidazolidinone/AlCl₃ baths, *Electrochim. Acta*, 2014, **137**(8), p 470.
29. H. Wu, Y. Wu, M. Yan et al., Microstructure and mechanical properties of surface coating prepared on grade 2 titanium by Ni-B composite electroplating and laser cladding, *Opt. Laser Technol.*, 2023, **164**, 109498
30. Y. Li, P. Song, W. Wang et al., Microstructure and wear resistance of a Ni-WC composite coating on titanium grade 2 obtained by electroplating and electron beam remelting, *Mater Charact*, 2020, **170**, 110674
31. Z. Lin, S. Dabakhsh and A. Rashid, Developing processing windows for powder pre-heating in electron beam melting, *J. Manuf. Process.*, 2022, **83**, p 180–191.
32. B. Hallstedt, M. Noori, F. Kies et al., Thermodynamic database for multi-principal element alloys within the system Al-Co-Cr-Fe-Mn-Ni-C, *Calphad*, 2023, **83**, 102644
33. J.W. Yeh, S.K. Chen, S.J. Lin et al., Nanostructured high-entropy alloys with multiple principal elements: novel alloy design concepts and outcomes, *Adv. Eng. Mater.*, 2004, **6**(5), p 299–303.
34. T. Dong, P. Lu, Q. Ma et al., Effect of laser remelting on high-temperature oxidation resistance of AlCoCrFeNi high-entropy alloy coating, *Surf. Coat. Technol.*, 2023, **466**, 129608
35. W.R. Wang, W.L. Wang and J.W. Yeh, Phases, microstructure and mechanical properties of Al_xCoCrFeNi high-entropy alloys at elevated temperatures, *J. Alloys Compd.*, 2014, **589**, p 143–152.
36. R.T. Foley, M.B. Peterson and C. Zapf, Frictional characteristics of cobalt, nickel, and iron as influenced by their surface oxide films, *ASLE Trans.*, 1963, **6**(1), p 29–39.

Publisher's Note Springer Nature remains neutral with regard to jurisdictional claims in published maps and institutional affiliations.

Springer Nature or its licensor (e.g. a society or other partner) holds exclusive rights to this article under a publishing agreement with the author(s) or other rightsholder(s); author self-archiving of the accepted manuscript version of this article is solely governed by the terms of such publishing agreement and applicable law.